doi:10.1016/j.jmb.2010.10.003 J. Mol. Biol. (2010) 404, 478–492

Contents lists available at www.sciencedirect.com

Journal of Molecular Biology

journal homepage: http://ees.elsevier.com.jmb

Alternative Oligomeric States of the Yeast Rvb1/Rvb2 Complex Induced by Histidine Tags

Kevin L. Y. Cheung[1], Jennifer Huen[2], Yoshito Kakihara[2], Walid A. Houry[2] and Joaquin Ortega[1]*

[1]*Department of Biochemistry and Biomedical Sciences and M. G. DeGroote Institute for Infectious Diseases Research, Health Sciences Center, McMaster University, 1200 Main Street West, Hamilton, Ontario, Canada L8N 3Z5*
[2]*Department of Biochemistry, University of Toronto, Toronto, Ontario, Canada M5S 1A8*

Received 17 August 2010; received in revised form 14 September 2010; accepted 1 October 2010
Available online 8 October 2010

Edited by W. Baumeister

Keywords:
AAA+;
electron microscopy;
helicase;
pontin;
reptin

Rvb1 and Rvb2 are essential AAA$^+$ (*A*TPases *a*ssociated with diverse cellular *a*ctivities) helicases, which are important components of critical complexes such as chromatin remodeling and telomerase complexes. The oligomeric state of the Rvb proteins has been controversial. Independent studies from several groups have described the yeast and human Rvb1/Rvb2 complex both as a single and as a double hexameric ring complex. We found that histidine-tagged constructs of yeast Rvb proteins employed in some of these studies induced the assembly of double hexameric ring Rvb1/Rvb2 complexes. Instead, untagged versions of these proteins assemble into single hexameric rings. Furthermore, purified endogenous untagged Rvb1/Rvb2 complexes from *Saccharomyces cerevisiae* were also found as single hexameric rings, similar to the complexes assembled *in vitro* from the purified untagged components. These results demonstrate that some of the differences between the reported structures are caused by histidine tags and imply that further studies on the purified proteins should be carried out using untagged constructs.

Introduction

Rvb1 and Rvb2 are two highly conserved homologous proteins that belong to the AAA$^+$ (*A*TPases *a*ssociated with diverse cellular *a*ctivities) family of ATPases. Rvb1 was first identified as part of a complex with TATA box binding protein,[1,2] and Rvb2 as part of a complex involved in c-Myc-mediated cell transformation in HeLa cells.[3] Since then, these two proteins have been found as components of a large number of complexes that carry out many distinct functions in a variety of molecular pathways, including chromatin remodeling,[4–7] assembly and maturation of small nucleolar ribonucleoproteins,[8–11] and mitosis.[12,13]

The X-ray structure of human Rvb1[14] and the electron microscopy (EM) structures of both human[15] and yeast[16,17] Rvb1/Rvb2 complexes have been reported. In the crystal structure of human Rvb1, the protein assembles as a single hexameric ring (Fig. 1). Each monomer in the ring has three distinct domains: DI, DII, and DIII. The first and last domains constitute the AAA$^+$ core domain, which contains the predicted elements of the AAA$^+$ module for nucleotide binding and hydrolysis (Walker A, Walker B, sensor 1, and sensor 2 motifs). DII is a 170-amino-acid stretch intercalated within DI (Fig. 1). Therefore, this domain is also known as the 'insertion' domain, and it has been proposed to be important for DNA/RNA binding.[14] The insertion domain is attached to DI by a linker region composed of two β-strands,

*Corresponding author. E-mail address: ortegaj@mcmaster.ca.

Abbreviations used: EM, electron microscopy; BN, Blue native; 3D, three-dimensional; TEV, tobacco etch virus; 2D, two-dimensional; PDB, Protein Data Bank; EMDB, Electron Microscopy Data Bank.

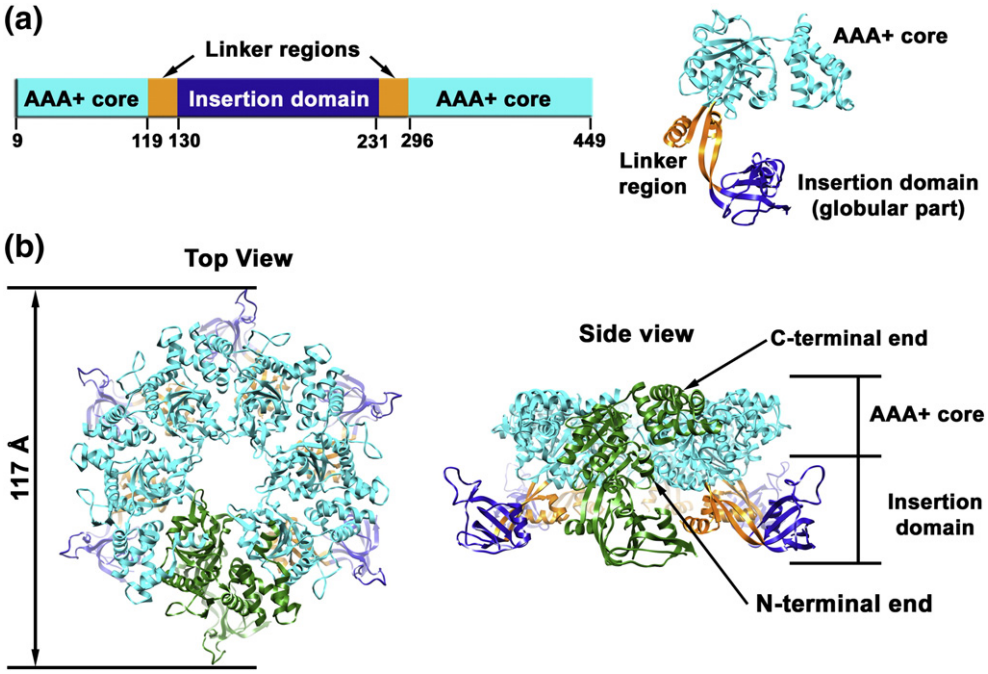

Fig. 1. X-ray structure of the human Rvb1 protein. (a) Linear diagram (left) of the human Rvb1 protein indicating the locations of the AAA^+ core domains and the globular part of the insertion domain. The linker regions between the two domains are indicated. Residues delimiting all these domains are also indicated in the diagram. On the right, the X-ray structure of the human Rvb1 monomer is shown as a ribbon representation. The domains of the protein are color coded as in the linear diagram. (b) Top view (left) and side view (right) of the hexameric ring formed by the human Rvb1 protein as a ribbon representation color coded as in (a), except for one of the monomers, which is shown in green. The AAA^+ core domains, the globular parts of the insertion domains in the hexameric ring, and the N-terminal and C-terminal ends of the monomer are shown in green. Images in (a) and (b) were prepared from PDB ID 2C9O.

which probably allows for the movement of this domain with respect to DI.

There have been a number of groups reporting also on the architecture of the human and yeast Rvb1/Rvb2 complexes using EM. In spite of the high degree of homology among human and yeast proteins, there are significant differences observed among published structures. Contradictions are observed not only between the reconstruction of the human complex and the two structures reported for the yeast Rvb1/Rvb2 complex but also among the two yeast assemblies.

One of these studies[15] showed that the structure of the human Rvb1/Rvb2 complex assembled as a double hexameric ring (Fig. 2a). Recently, an additional publication reported that this complex forms single and double hexamers, as well as smaller oligomeric forms.[18] Subsequently, two independent groups published structural information on the yeast Rvb1/Rvb2 complex. Our group[16] concluded that yeast Rvb1 and Rvb2 assemble into single hexameric rings containing both proteins (Fig. 2b). Surprisingly, a second study[17] revealed that the same complex organizes as an asymmetric double-ring dodecamer with top and bottom compact hexameric rings occupied by the DI and DIII domains of the Rvb proteins. Six protein densities project from the rings towards the center of the structure, forming two layers of discontinuous density (equatorial domains) and leaving lateral openings to an internal chamber in the structure. The equatorial domains are made of intercalated DII domains interacting in the middle of the structure and maintaining the integrity of the dodecameric structure (Fig. 2c). Interestingly, this last study suggests that the dodecamer is composed of two homohexamers, each containing only one of the proteins. Nevertheless, a conclusion that can be drawn from the comparison of the three structures[19] is that, in spite of the double-ring or single-ring structure adopted by the Rvb1 and Rvb2 proteins in the different studies, there is a reasonable degree of compatibility between the X-ray structure of the human Rvb1[14] and the two structures reported for the yeast complex.[16,17] However, the EM reconstruction of the human Rvb1/Rvb2 complex[15] disagrees with the published yeast EM structures or the human X-ray structure.

The different structural assemblies observed for Rvb1/Rvb2 may reflect that these proteins can assemble into multiple oligomeric states and might undergo a multitude of conformational changes while performing their functions. Accordingly, the reported structures may represent the different functional states of the Rvb1/Rvb2 complex. However, a comparison of the approaches used to

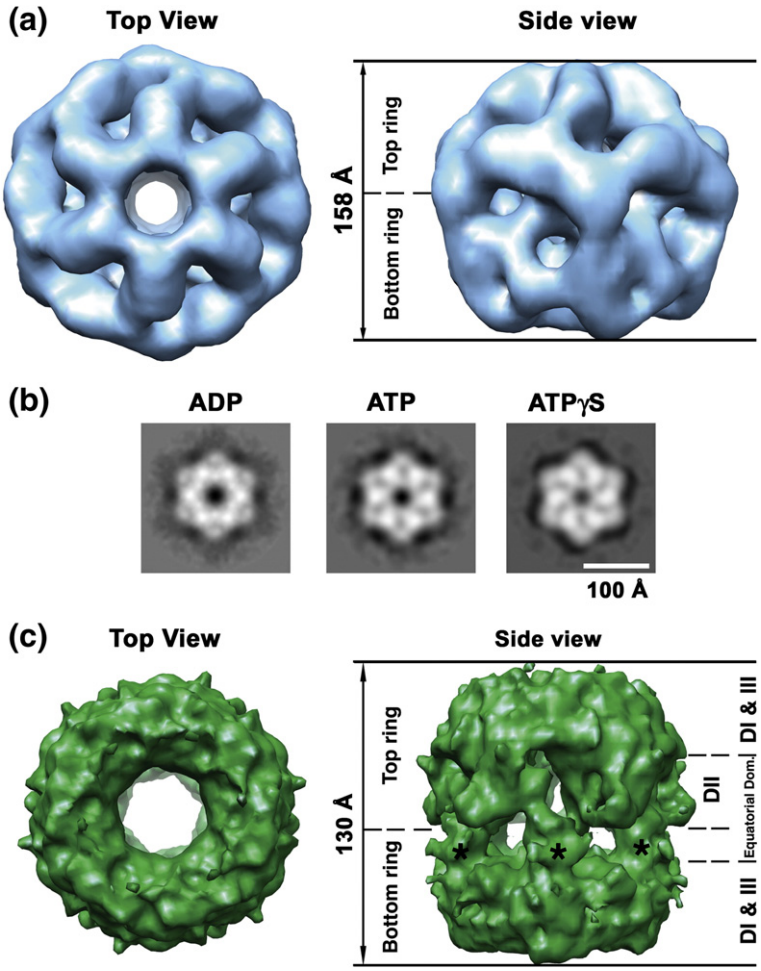

Fig. 2. Available EM structures of the human and yeast Rvb1/Rvb2 complex. (a) Top and side views of the 3D reconstruction of the human Rvb1/Rvb2 complex obtained from negatively stained electron micrographs. The images were prepared from EMDB ID 1317. (b) Two-dimensional averages of the yeast Rvb1/Rvb2 complex in the presence of three different nucleotide states. (c) Surface-rendering representation of the 3D reconstruction of the yeast Rvb1/Rvb2 complex obtained by cryo-EM. A top view and a side view are shown. Asterisks indicate the projected densities from the bottom ring into the equatorial domain; the locations of DI, DII, and DIII are indicated. The images were prepared from EMDB ID 2865.

produce these structures red flagged some experimental aspects that could be causing the observed differences.[19] Therefore, we tested the effects of some of the experimental conditions differing among the studies cited to determine their effects on the oligomeric state of the Rvb1/Rvb2 complex.

In particular, several of the studies on the human[14,15] and yeast Rvbs[17] used histidine or FLAG-tagged versions of these proteins to assemble the Rvb1/Rvb2 complex. Here, we show that histidine-tagged yeast Rvb1 and Rvb2 proteins form oligomers larger than the hexamers formed by the untagged versions of these proteins, both by themselves and when combined in an assembly reaction to form Rvb1/Rvb2 complexes. We found that these larger oligomers are dodecamers composed of two stacked hexameric rings in a DII–DII configuration and that they reverted to single hexameric rings upon removal of the histidine tags.

In addition, most of the published structural studies[15,16] assembled the Rvb1/Rvb2 complex *in vitro* from purified components expressed in *Escherichia coli*. However, one study performed the complex assembly *in vivo* through coexpression of both Rvb1 and Rvb2 proteins in insect cells.[17] To test the effect of the protein expression system and whether *in-vivo*-assembled untagged Rvb1/Rvb2 complexes form double or single hexameric rings, we purified the endogenous untagged Rvb1/Rvb2 complex from *Saccharomyces cerevisiae*. We found that such isolated complexes are single hexameric rings that are structurally similar to the ones obtained *in vitro* from purified untagged Rvb proteins expressed in *E. coli*. Therefore, we concluded that the protein expression system and whether the complexes were assembled *in vivo* or *in vitro* did not have an effect on the oligomeric state of the Rvb1/Rvb2 complex. However, it is important that further studies on purified Rvb1/Rvb2 complexes are carried out with untagged constructs.

Results

Histidine-tagged Rvb1 and Rvb2 proteins form larger oligomers compared to the untagged proteins

To determine whether the presence of histidine tags in the yeast Rvb1 or Rvb2 proteins has any effect

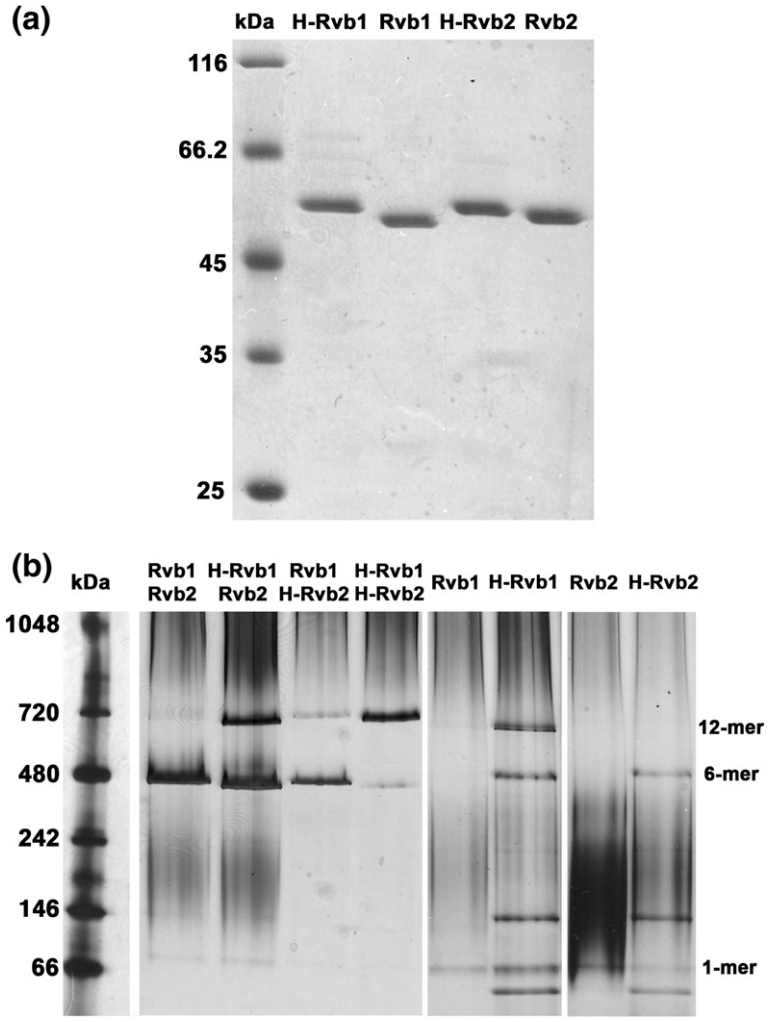

Fig. 3. N-terminal histidine tags in the Rvb1 and Rvb2 proteins induce the formation of oligomeric forms larger than hexamers. (a) Purified untagged and N-terminal His_6-tagged fusion versions of the Rvb1 and Rvb2 proteins were resolved in a 12% SDS-PAGE gel and stained by Coomassie brilliant blue. Proteins containing an N-terminal His_6-tag are denoted with an "H" label before the name of the protein. (b) Untagged (Rvb1/Rvb2), singly tagged (H-Rvb1/Rvb2 and Rvb1/H-Rvb2), and doubly tagged (H-Rvb1/H-Rvb2) complexes were assembled in the presence of 1.5 mM ADP, resolved in a BN-PAGE gel, and stained with silver staining. The untagged and histidine-tagged versions of the Rvb1 and Rvb2 proteins were also resolved in these gels. The bands corresponding to the dodecamers (12-mer), hexamers (6-mer), and monomers (1-mer) are indicated.

on the oligomeric state adopted by the assembled Rvb1/Rvb2 complex, we expressed and purified both untagged and N-terminal His_6-tagged fusion versions of the Rvb1 and Rvb2 proteins (Fig. 3a).

Subsequently, the untagged (Rvb1/Rvb2), singly histidine-tagged (His-Rvb1/Rvb2 and Rvb1/His-Rvb2), and doubly histidine-tagged (His-Rvb1/His-Rvb2) complexes were assembled in reaction mixtures containing equimolar amounts of both proteins. The oligomeric state of the complexes was assessed using Blue native (BN) PAGE. The sample containing the untagged Rvb1/Rvb2 complex showed mainly one band with mobility similar to that of the 480-kDa molecular mass marker (Fig. 3b). The theoretical molecular masses of Rvb1 and Rvb2 are 50.5 and 51.6 kDa, respectively, and our previous work[16] established that the untagged proteins form 300-kDa hexameric rings. Therefore, this band represents hexameric Rvb1/Rvb2 complexes. The slightly slower mobility of these assemblies is explained because migration in native polyacrylamide gels is dictated not only by the molecular weight but also by the shape of

Fig. 4. Purification and visualization of the untagged, singly histidine-tagged, or doubly histidine-tagged Rvb1/Rvb2 complexes by EM. (a) Elution profile of the untagged, singly histidine-tagged, and doubly histidine-tagged Rvb1 and Rvb2 complexes from a Superdex 200 column. In all cases, the size-exclusion chromatography column was equilibrated with a buffer containing 1.5 mM ADP. Proteins containing an N-terminal His_6-tag are denoted with an "H" label before the name of the protein. The arrows in the elution profiles indicate the expected elution volume for the dodecamers (9.8 mL), hexamers (11.3 mL), and monomers (15.2 mL). Samples were withdrawn from the fractions between 10 and 12 mL, resolved in a 12% SDS-PAGE gel, and stained with Coomassie brilliant blue. (b) Representative negative-staining electron micrographs of purified untagged, singly histidine-tagged, and doubly histidine-tagged Rvb1/Rvb2 complexes obtained from fractions between 10 and 12 mL from the elution profiles in (a). (c) Two-dimensional averages of untagged, singly histidine-tagged, and doubly histidine-tagged Rvb1/Rvb2 complexes obtained from particle images selected from electron micrographs obtained from fractions between 10 and 12 mL from the elution profiles in (a).

the complexes. Surprisingly, in the samples containing the singly and doubly histidine-tagged complexes, we observed an additional prominent band of similar mobility to the 720-kDa molecular mass marker. We hypothesized that this band corresponds to a dodecameric complex formed presumably by two stacked hexameric rings. The proportion of hexamers and putative dodecamers was not constant in the three samples. Hexamers were more abundant in the sample containing the Rvb1/His-Rvb2

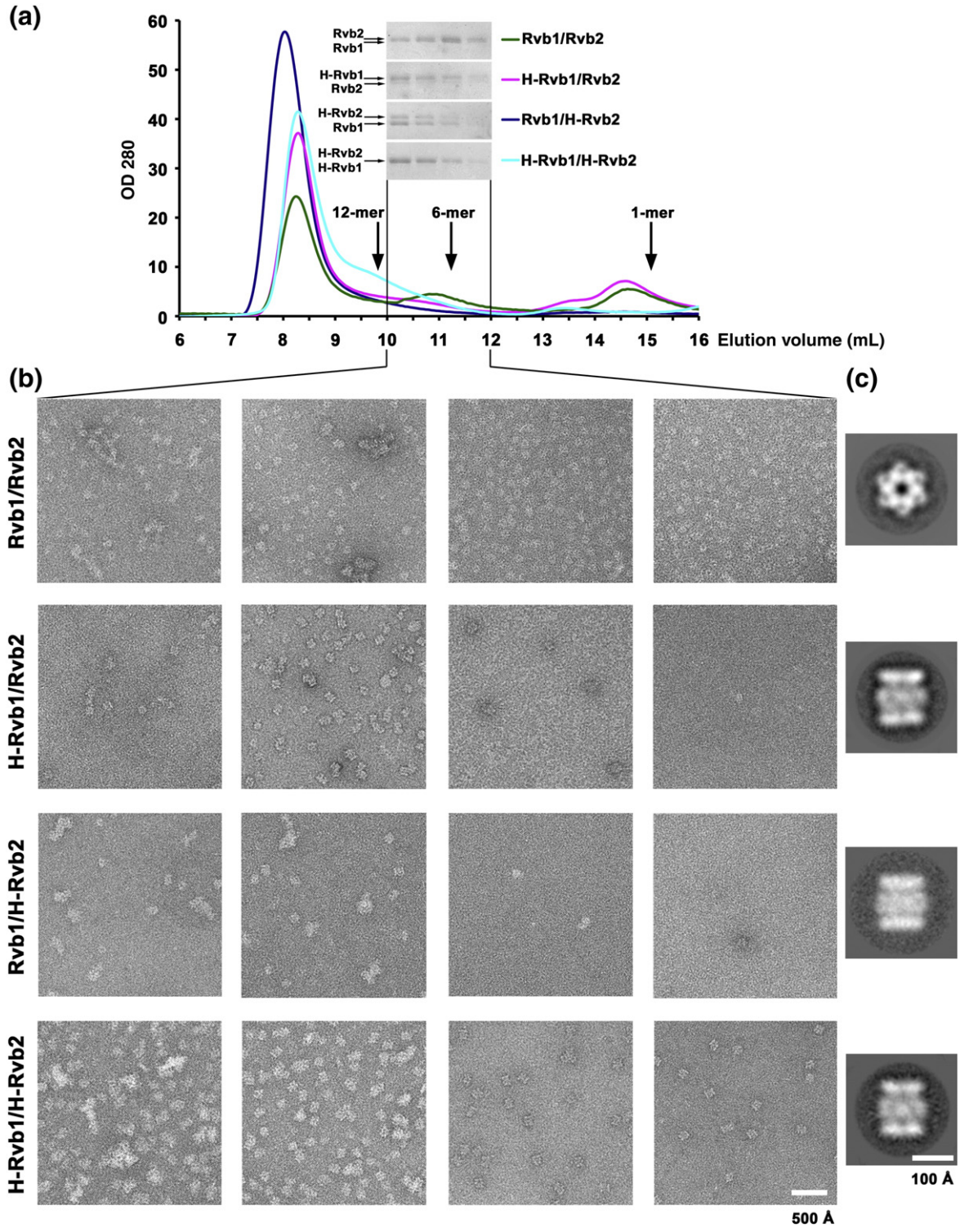

Fig. 4 *(legend on previous page)*

complex; however, hexamers coexisted in similar amounts with the putative dodecamers in the His-Rvb1/Rvb2 complex. In the sample containing His-Rvb1/His-Rvb2 complexes, the larger oligomeric form was predominant (Fig. 3b). It is important to note that the band representing putative dodecamers in the sample containing untagged complexes, although visible, was very faint (Fig. 3b), implying that the proportion of dodecamers in that sample was extremely small (<1%).

Both untagged Rvb1 and Rvb2 alone resolved as a single band of similar mobility to the 66-kDa molecular mass marker, consistent with the monomeric state of these proteins in solution.[16] The lane containing untagged Rvb2 also showed a smear probably representing a heterogeneous mixture of oligomers smaller than hexamers. In contrast, loading either N-terminal His_6-Rvb1 or N-terminal His_6-Rvb2 produced multiple bands in the native polyacrylamide gel. In particular, the first protein showed two distinct bands corresponding to the hexameric and putative dodecameric forms, as well as multiple bands at lower molecular weights. N-terminal His_6-Rvb2 produced a similar pattern, but the band corresponding to the putative dodecamers was absent (Fig. 3b). These data clearly indicate that the presence of N-terminal histidine tags in the Rvb1 and Rvb2 proteins further promotes the formation of large oligomers that are only faintly observed with the untagged complex.

Visualization of the oligomers formed by the histidine-tagged Rvb1 and Rvb2 proteins by EM

To structurally characterize the larger oligomeric forms observed with the N-terminal His_6-tagged fusion versions of the Rvb1 and Rvb2 proteins, we analyzed assembly reactions containing untagged, singly histidine-tagged, or doubly histidine-tagged Rvb1/Rvb2 complexes by size-exclusion chromatography and EM.

The sample containing untagged Rvb1/Rvb2 complexes resolved in three distinct peaks (Fig. 4a). A first peak, centered at an elution volume of 8.2 mL, corresponded to a very large and heterogeneous population of complexes as seen by negative-staining EM (data not shown), whereas a second peak, centered at an elution volume of 14.6 mL, was compatible with a population of monomers (~50 kDa). A third peak, centered at an elution volume of 11 mL, was broad and close to the expected elution volume of the Rvb1/Rvb2 hexamer (~300 kDa). Interestingly, this peak was only observed if the column had been previously equilibrated with a buffer containing 1.5 mM ADP. Fractions from this peak (10–12 mL) contained approximately equimolar amounts of both proteins, were applied to EM grids, and were observed under negative-staining conditions (Fig. 4b). The fraction closer to the peak centered at an elution volume of 8.2 mL still showed a mainly heterogeneous mixture of protein complexes. However, the other fractions revealed large amounts of ring-shaped particles, which our previous study determined as representing the top views of single hexameric Rvb1/Rvb2 complexes.[16] An average image calculated from ~500 particles also confirmed the similarity of this oligomeric form to the single hexameric rings characterized in our previous study (Fig. 4c).

All samples containing the singly and doubly histidine-tagged Rvb1/Rvb2 complexes produced an elution profile with a large peak, centered at an elution volume of 8 or 8.2 mL, containing mainly large heterogeneous complexes (data not shown). Only the sample containing the His-Rvb1/Rvb2 complex showed an additional smaller peak at the expected elution volume for monomers of the Rvb proteins (Fig. 4a). Differently from the sample containing the untagged Rvb1/Rvb2 complex, the three histidine-tagged complexes produced the same profiles regardless of the presence or the absence of ADP in the buffer used to equilibrate the column (data not shown). Importantly, any of the profiles showed a prominent peak at the expected elution volume for a hexamer or a dodecamer (~600 kDa). However, the large peak in the three samples showed a tail extending towards higher elution volumes, and this feature was most predominant in the profile of the His-Rvb1/His-Rvb2 sample. Fractions from this tail corresponding to the expected elution volumes between the dodecamer and the hexamer (10–12 mL) contained approximately equimolar amounts of both proteins and were visually inspected under negative-staining conditions (Fig. 4b). Similarly to the untagged Rvb1/Rvb2 complex, the fraction closer to the large peak still contained mainly large heterogeneous aggregates. However, the subsequent fractions contained a few ring-shaped particles and mainly barrel-shaped particles with three parallel striations. The images of the barrel-shaped particles from each histidine-tagged sample were selected and averaged, confirming that these oligomeric forms are structurally very different from the one observed with the untagged Rvb1/Rvb2 complex (Fig. 4c).

The histidine-tagged Rvb1/Rvb2 complexes assemble as double hexameric ring structures

To obtain a better description of the oligomers formed by the singly and doubly histidine-tagged Rvb1/Rvb2 complexes, we obtained their three-dimensional (3D) reconstruction using single-particle approaches and electron micrographs prepared from column fractions containing the highest concentration of purified complexes (Fig. 4).

To this end, several thousands of barrel-shaped particles and a few hundred ring-shaped particles

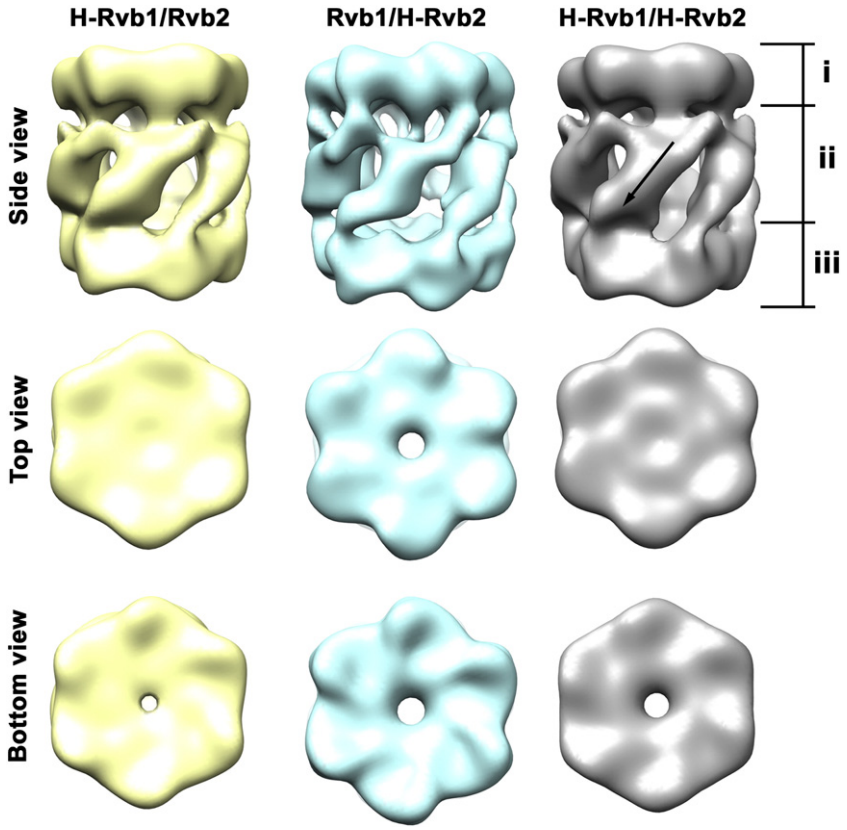

Fig. 5. Three-dimensional reconstructions of the histidine-tagged Rvb1/Rvb2 complexes. Side, top, and bottom views of the EM structures of the three histidine-tagged Rvb1/Rvb2 complexes. EM maps are shown with a surface-rendering representation using a threshold value representing approximately 100% of their estimated mass (~600 kDa). The three layers of density into which the EM maps are divided are indicated in one of the side views. The arrow on the same map indicates one of the densities projecting from the top ring and running through the middle layer in an oblique fashion.

representing the side and top views of the complexes, respectively, were selected for the three histidine-tagged Rvb1/Rvb2 complexes. Initially, the ring-shaped particles were analyzed with algorithms capable of detecting rotational symmetries,[20] which found that these complexes had 6-fold symmetry. No other order of symmetry was found to be statistically significant. Results for Student's *t* test and the spectral ratio product are shown in Table S1 and formally establish the symmetry of the three histidine-tagged Rvb1/Rvb2 complexes.

Only the barrel-shaped particles (~10,000 particles for each complex) were used to obtain the 3D volumes. These views ensure that single hexameric rings that may also be present in the sample are not used in the reconstruction process. The reconstructions of the three complexes were calculated by the projection-matching approach. To rule out any model bias in the resulting structures, we used several initial models, including the previously published double hexameric ring structure of the yeast Rvb1/His-Rvb2 complex,[17] and constructed a reference volume using the average of the top views, side views, and 6-fold symmetries detected in the rotational symmetry analysis.[21] In addition, the 3D reconstruction process was performed both by assuming the 6-fold symmetry (*c*6) and by treating these structures as asymmetric objects (*c*1). Regardless of the initial map and the symmetry imposed during the refinement process, we consistently obtained essentially the same 3D reconstruction for each complex.

The 3D reconstructions of the three histidine-tagged Rvb1/Rvb2 complexes at ~20 Å resolution (Fig. S1) show a cylindrical structure with a diameter of ~114 Å and a height of 142 Å (Fig. 5). The Rvb1/His-Rvb2 and His-Rvb1/His-Rvb2 complexes were slightly longer than the His-Rvb1/Rvb2 complex probably due to the different amount of flattening experienced during the preparation of the negative-staining grids or due to the genuine conformational differences between the complexes. Inspected from the side, these reconstructions present three different layers of density (i, ii, and iii). The two outer layers (i and ii) are denser than the one in the middle (ii) and most likely comprise the core AAA^+ domains of the Rvb proteins assembled as hexameric rings. The middle layer is less dense and probably contains the insertion domains of the Rvb proteins. This layer is made of six protein densities projecting from the top and bottom rings and run in an oblique fashion through the middle layer. The interactions of the densities in the middle layer with the top and bottom rings are different (Fig. 5, side view), and the two outer rings are also not identical (Fig. 5, top and bottom views). The asymmetry of the complex seems to be real, since all the 3D reconstructions

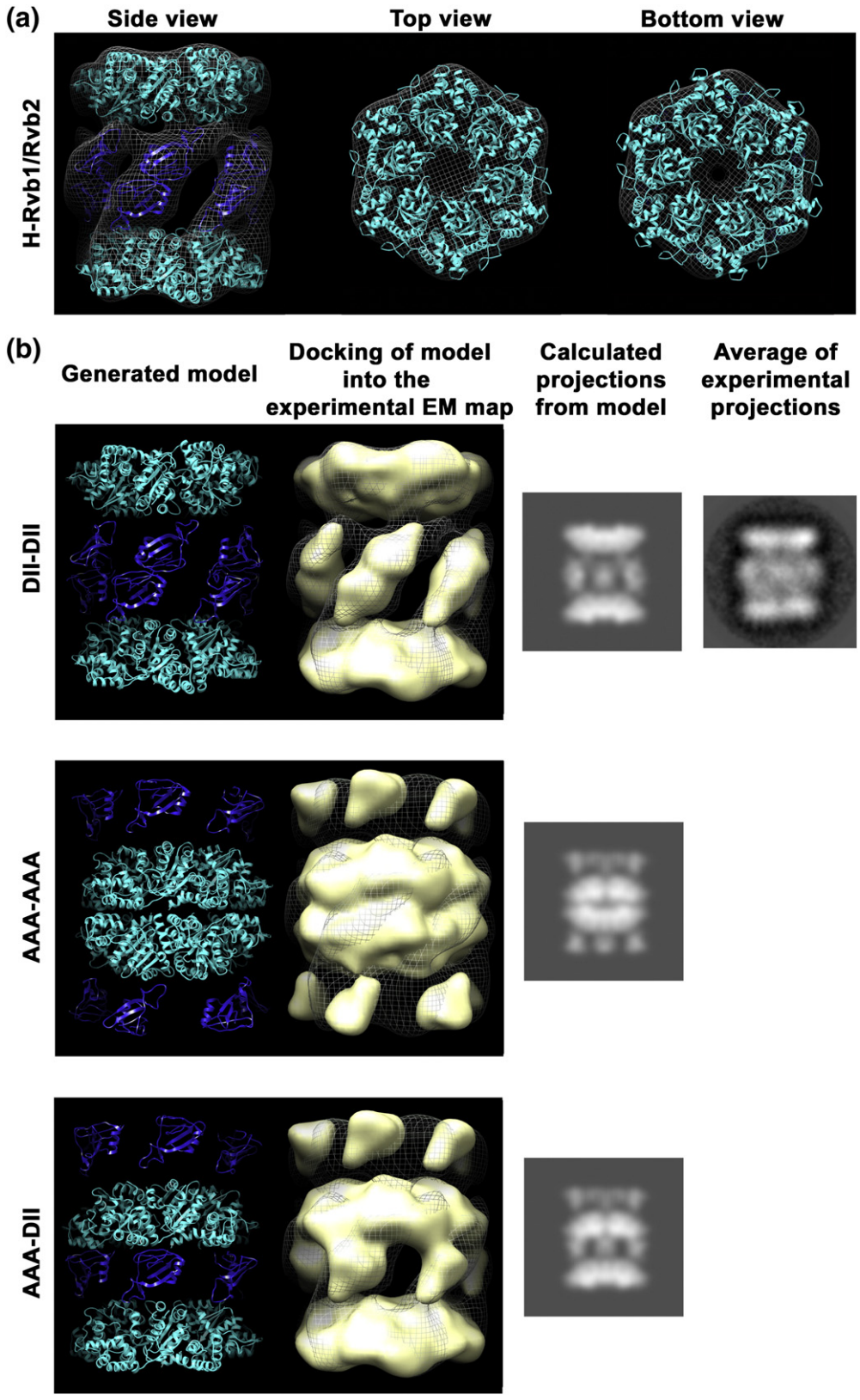

Fig. 6 *(legend on next page)*

diverged into an asymmetric structure in spite of the use of an initial reference with fully symmetric top and bottom rings (*d*6 symmetry). In addition, we noticed that, in the Rvb1/His-Rvb2 complex, the densities in the middle layer connect to the outer rings in a slightly different pattern. Altogether, these results show that the histidine-tagged Rvb1/Rvb2 complexes assemble as dodecameric structures composed of two stacked hexameric rings.

The dodecameric structures formed by the histidine-tagged Rvb1/Rvb2 complexes are consistent with a DII–DII stacking of the two hexameric rings

Next, we examined whether the 3D structures obtained for the histidine-tagged Rvb1/Rvb2 complexes were consistent with a DII–DII, AAA–AAA, or AAA–DII stacking of the two hexameric rings. To this end, we used the X-ray structure of human Rvb1 to perform docking experiments on our EM maps.

Initially, we observed that the entire X-ray structure of the human Rvb1 hexamer[14] fits the EM maps poorly, suggesting that the relative orientations of the AAA^+ core domain and of the insertion domain are different between the crystal structure and the EM structure (Fig. S2). In the crystal structure, the relative orientation between the two domains is dictated by a linker region (residues 120–129 and 232–295) (Fig. 1a), which probably adopts a different conformation in the two structures. Consequently, this linker region of the human Rvb1 structure was not included in our docking experiments, and the AAA^+ core domain (residues 9–119 and 296–449) and the globular part of the insertion domain (residues 130–231) (Fig. 1a) were docked independently onto the EM density maps by rigid-body fitting. The AAA^+ core domains of the two Rvb1 hexameric rings fit unambiguously the two outer layers of density (Fig. 6a, top; Fig. S3a and b, top), and two insertion domains, each from one ring, docked well onto each of the six protein densities in the middle layer of the EM maps. However, due to the limited resolution of the 3D reconstructions, it was possible to fit the pairs of insertion domains in more than one orientation. Therefore, we arbitrarily chose the orientation proposed by Torreira *et al.*, which was also shown as a possible local optimum in our docking experiments (Fig. 6a, top; Fig. S3a and b, top).[17] The good agreement found between the crystal structure of the Rvb1 hexamer and our EM density maps suggested that the histidine-tagged complexes are formed by two stacked hexameric rings arranged in a DII–DII configuration in which the insertion domains from the hexamers interact at the equator of the complex.

To ensure that the models generated agree with the observed experimental projections of the histidine-tagged complexes, we generated side-view projections limited to the resolution of the EM maps (~20 Å) from the DII–DII models and compared them with the average of experimental projections from the corresponding complexes (Fig. 6b, top; Fig. S3a and b, bottom). The region connecting the AAA^+ core domains with the insertion domains was less dense in the calculated projections from the models, since the linker region between the two domains was not used for the docking experiments. Nonetheless, an excellent match between the calculated projections and the experimental average was obtained for the three histidine-tagged complexes (Fig. 6b, top; Fig. S3a and b, bottom).

To prove that the 3D reconstructions obtained were inconsistent with AAA–AAA and AAA–DII stacking of the hexameric rings, we also constructed these two additional models and calculated their side-view projections. Both configurations were modeled from the DII–DII model of the His-Rvb1/Rvb2 complex. The AAA–AAA model was made by inverting the two Rvb1 hexameric rings such that the AAA^+ core domains were then accommodated in the middle layer of density on the EM maps. In this configuration, the insertion domains project from each ring towards the outer layers of density (Fig. 6b, middle, left column). Similarly, the AAA–DII model was assembled by placing one of the Rvb1 rings as in the DII–DII model and by inverting the second ring and orienting it as in the AAA–AAA

Fig. 6. Docking of the X-ray structure of the human Rvb1 hexamer onto the 3D reconstruction of the histidine-tagged Rvb1/Rvb2 complexes. (a) The fitting of the AAA^+ core domain and the globular part of the insertion domains of the crystal structure of human Rvb1 into the 3D reconstruction of the His-Rvb1/Rvb2 complex. The AAA^+ core domain and the insertion domains are shown as a ribbon representation color coded as in Fig. 1 and prepared from PDB ID 2C9O. The EM density map of the His-Rvb1/Rvb2 complex is shown as a mesh. (b) Layout of the two Rvb hexamers in the histidine-tagged Rvb1/Rvb2 complexes. The left column shows the DII–DII, AAA–AAA, and AAA–DII models generated for the dodecameric Rvb1/Rvb2 complex indicating three possible configurations of the two hexameric rings. The models were generated by fitting the crystal structure of human Rvb1 into the 3D reconstruction of the His-Rvb1/Rvb2 complex in different orientations. The AAA^+ core domain and the insertion domains are shown as a ribbon representation color coded as in Fig. 1. The second column from the left shows the surface-rendering representation of the density maps generated from the models fitted onto the density map of the 3D reconstruction of the His-Rvb1/Rvb2 complex represented as a mesh. The third column from the left shows the calculated side-view projections from the models, and the right column displays an average of experimental projections from the His-Rvb1/Rvb2 complex obtained from negatively stained electron micrographs.

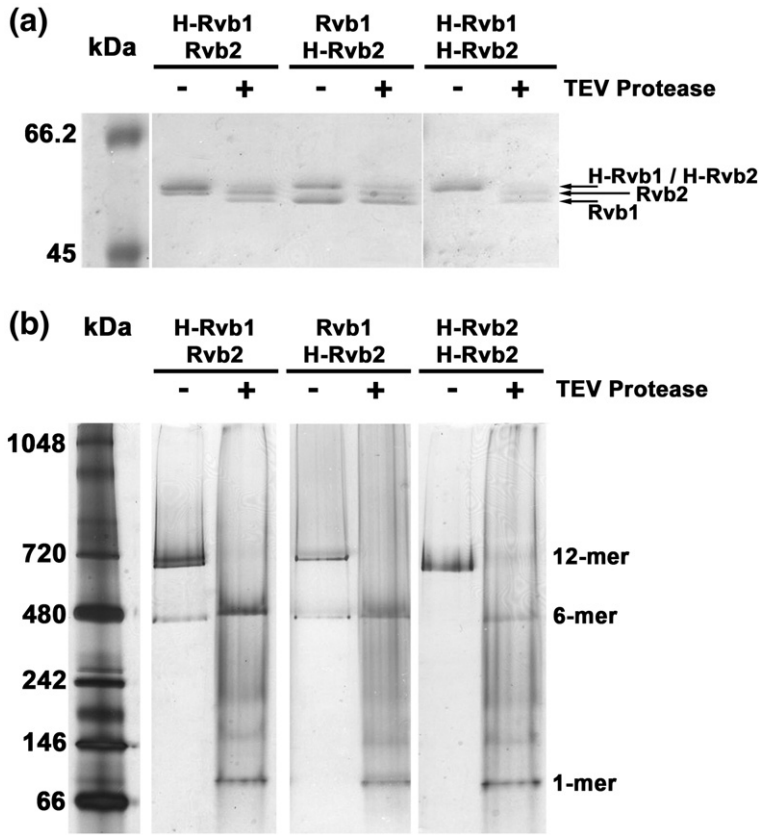

Fig. 7. Cleavage of histidine tags dissociates the dodecamers formed by the Rvb1/Rvb2 complexes into hexamers. (a) Singly and doubly histidine-tagged Rvb1/Rvb2 complexes were purified by size-exclusion chromatography. A 50-μL sample of the fraction containing the complexes was treated with 5 μL of a 6 mg/mL stock of TEV protease to remove the histidine tags. A 7-μL volume of the reaction containing TEV-treated and untreated complexes was mixed with an equal volume of a 2× concentrated loading buffer, resolved in a 12% SDS-PAGE gel, and stained by Coomassie brilliant blue. Proteins containing an N-terminal His_6-tag are denoted with an "H" label before the name of the protein. Arrows on the right side of the gel indicate the identity of the protein bands. (b) A 15-μL volume of each reaction containing a TEV-treated Rvb1/Rvb2 complex or an untreated Rvb1/Rvb2 complex was mixed with 5 μL of loading dye, resolved in a BN-PAGE gel, and stained with silver staining. The bands corresponding to the dodecamers (12-mer), hexamers (6-mer), and monomers (1-mer) are indicated.

model, such that the insertion domains of one ring interact with the AAA^+ core domain of the second ring at the equator of the complex (Fig. 6b, bottom, left column). The density maps generated from both models fitted the experimental EM map of the His-Rvb1/Rvb2 complex very poorly (Fig. 6b, middle and bottom, middle column). Similarly, the calculated side-view projections from both models were inconsistent with the experimental projections (Fig. 6b, middle and bottom, right column).

The absolute handedness of the EM maps was not determined. Therefore, we also docked the X-ray structure of the Rvb1 hexamer onto the His-Rvb1/Rvb2 EM map with opposite handedness and built the alternative DII–DII model (Fig. S4, top). The calculated side-view projections from this model were also very similar to the average of experimental projections from His-Rvb1/Rvb2 (Fig. S4, bottom). In addition, because the orientation of the insertion domains for the construction of the DII–DII models was chosen arbitrarily, additional DII–DII models were also constructed with an alternative orientation for these domains. In this case, we also found an excellent agreement between the calculated projections and the experimental projections (data not shown).

These results confirm that the 3D reconstructions obtained for the histidine-tagged Rvb1/Rvb2 complex are all consistent with a DII–DII configuration of the two hexameric rings but also incompatible with the other configurations.

The histidine-tag-induced dodecamer formed by the Rvb1/Rvb2 complexes is reversible

We tested whether the histidine-tag-induced dodecamers of the Rvb1/Rvb2 complexes remained stable after the removal of the tag. Singly and doubly histidine-tagged Rvb1/Rvb2 complexes were purified by size-exclusion chromatography and treated with tobacco etch virus (TEV) protease to remove the histidine tags. Removal of the tags was monitored by SDS-PAGE (Fig. 7a). The N-terminal His_6-tagged fusion versions of the Rvb1 and Rvb2 proteins run very similarly in SDS-PAGE; thus, only one band is seen in the lane containing an untreated His-Rvb1/His-Rvb2 complex (Fig. 7a). Cleavage was almost complete for the His-Rvb1/Rvb2 and His-Rvb1/His-Rvb2 complexes; however, it only reached ~60% in the Rvb1/His-Rvb2 complex.

Both TEV-treated and untreated complexes were loaded into a native gel (Fig. 7b). The untreated histidine-tagged Rvb1/Rvb2 complexes showed mainly a band of similar mobility to the 720-kDa molecular mass marker, representing the dodecameric

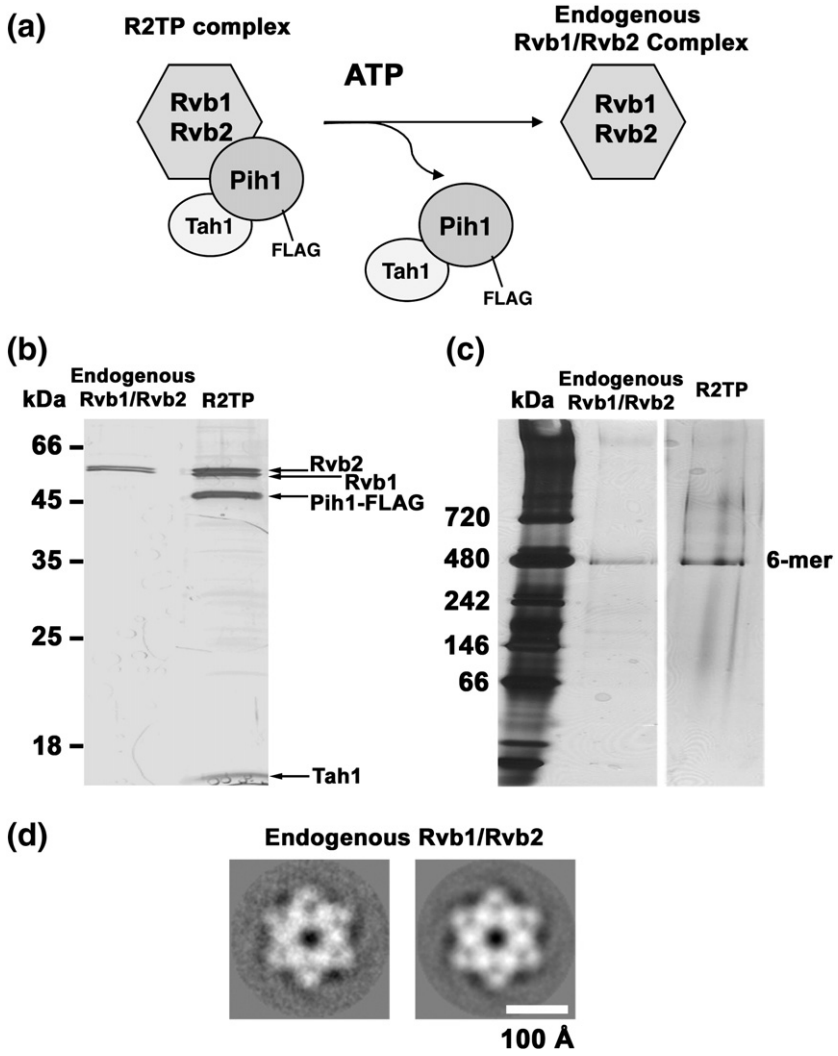

Fig. 8. Untagged endogenous Rvb1/Rvb2 complexes form single hexameric rings. (a) Cartoon representing the R2TP complex purified from *S. cerevisiae* containing a chromosomal copy of Pih1 3FLAG replacing the wild-type gene. The four protein components of the complex and the location of the FLAG tag are indicated. The cartoon also represents the dissociation of the Tah1 and Pih1 FLAG proteins from the endogenous Rvb1/Rvb2 complex upon incubation with ATP. (b) A 6-μL volume of purified R2TP and endogenous Rvb1/Rvb2 complexes was loaded into a 12% SDS-PAGE gel and stained by silver staining. The identity of the bands representing Pih1, Tah1, and the two Rvb proteins is indicated. (c) The two same samples (15 μL each) were mixed with 5 μL of loading dye, resolved in a BN-PAGE gel, and stained by silver staining. The bands corresponding to the hexameric complexes (6-mer) are indicated. (d) Two-dimensional average of an endogenous Rvb1/Rvb2 complex obtained from negatively stained particle images. The image on the left represents the 2D average, and the image on the right represents its 6-fold-symmetry version.

complexes, and a second band of faster mobility and significantly less intensity, representing hexamers. This second band was absent in the lane containing the untreated His-Rvb1/His-Rvb2 complex. Interestingly, the band representing the dodecameric complexes disappeared in the samples containing the Rvb1/Rvb2 complexes where the histidine tag had been removed.

It is important to note that, in all the untreated samples, the band corresponding to the dodecamers was predominant over the one representing the hexamers. This result is not in disagreement with the experiment shown in Fig. 3b because, in this case, size-exclusion chromatography fractions enriched in dodecameric complexes—instead of the full assembly reactions shown in Fig. 3b—were used.

These results imply that the histidine-tag-induced dodecamers formed by the Rvb1/Rvb2 complexes break down into hexamers upon the removal of the tags. Partial cleavage of the tags also causes a complete loss of the dodecameric structures, as seen with the sample containing TEV-treated Rvb1/His-Rvb2 complexes, suggesting that the histidine tags need to be present in most of the protein molecules to maintain the integrity of the dodecamers.

Purified endogenous Rvb1/Rvb2 complexes are single hexameric rings of similar structure to the *in-vitro*-assembled complexes with untagged Rvb proteins

In *S. cerevisiae*, the Hsp90 cofactors Pih1 and Tah1 interact with the Rvb1/Rvb2 complex to form the R2TP complex, which was shown to be important for mediating the assembly of small nucleolar ribonucleoproteins.[11,22] In this complex, Pih1 interacts directly with the Rvb1/Rvb2 complex, whereas Tah1 binds to Pih1 (Fig. 8a).[11] In order to image the endogenous *in-vivo*-assembled Rvb1/Rvb2 complex, we purified the R2TP complex using a yeast strain with an endogenously FLAG-tagged Pih1.[11] We found that the addition of ATP to the isolated complex results in the release of the Rvb1/Rvb2 complex from Tah1 and Pih1 (Fig. 8a and b). Both the

purified R2TP and the endogenous Rvb1/Rvb2 complexes were loaded into SDS-PAGE gels, to visualize protein content (Fig. 8b), and into native polyacrylamide gels, to analyze their oligomeric state (Fig. 8c). Interestingly, endogenously isolated Rvb1/Rvb2, both alone and in the context of the R2TP complex, ran as a single band corresponding to a single hexameric complex. No slower-mobility band representing dodecameric complexes was apparent.

The Rvb1/Rvb2 sample was visualized by negative-staining EM, revealing the presence of ring-shaped particles. An average image calculated from ~500 particles (Fig. 8d) confirmed the structural similarity of these oligomers to the single hexameric rings assembled *in vitro* from untagged Rvb proteins (Figs. 2b and 4c). Unfortunately, a 3D reconstruction of this complex (or of the *in-vitro*-assembled untagged Rvb1/Rvb2 complex) was not possible because the electron micrographs only provided top views of the Rvb1/Rvb2 single hexameric rings. Various treatments of the EM grids, such as floating the grids with polylysine[23] or glow discharging, failed to produce side-view projections of this complex (data not shown).

We also attempted to image the full R2TP complex; however, no additional densities were observed in the average image that could be assigned to the Pih1 and Tah1 proteins (data not shown). These proteins are rather small and might not be rigidly oriented with the complex. Nevertheless, these results indicate that the protein expression system and whether the complexes were assembled *in vivo* or *in vitro* did not have an effect on the oligomeric state of the Rvb1/Rvb2 complex.

Discussion

Recent attempts to understand the architecture of the Rvb1/Rvb2 complex have shown that Rvb1 and Rvb2 proteins organize into several types of assemblies. However, the use of the histidine-tagged constructs of these proteins in some of the studies has raised the question of whether the various described structures represent multiple functional states of the complex or are indeed induced by experimental conditions. We found that N-terminal His_6-tags in Rvb1 or Rvb2 proteins trigger the formation of double hexameric ring structures. The AAA^+ core domain of the Rvb proteins occupies the top and bottom of these structures, and the insertion domains are located at the equator, constituting the main area of interaction between the upper and the lower rings.

We do not know how the N-terminal His_6-tag in Rvb1 or Rvb2 leads to induction of double-ring structures. According to the model proposed here for the dodecamer, the N-terminal ends of the Rvb proteins locate at the base of the solid rings of density at the top and bottom of the structure and close to the insertion domains (Fig. 1b). Therefore, the N-terminal ends of the monomers in each ring are probably too far to induce the formation of the double-ring structure through a direct interaction between the N-terminal His_6-tags of one ring and the surface motifs in the monomers of the opposite ring. Similarly, a metal-mediated interaction between the N-terminal His_6-tags from opposite rings is also unlikely because of the distance separating both tags. A more plausible mechanism is that the presence of the N-terminal His_6-tags may induce a conformational change in the hexameric ring (probably in the insertion domains), allowing two rings to interact in a DII–DII fashion. This hypothesis is consistent with the reported dodecameric cryo-EM structure of the yeast Rvb1/Rvb2 complex assembled with untagged Rvb1 and the N-terminal histidine-tagged Rvb2 proteins,[17] where the two hexamers interact via the insertion domains. In addition, it is also in agreement with a recent study,[18] which used insertion domain deletion mutants of the human Rvb1 and Rvb2 proteins and showed that the insertion domain in Rvb1 seems to have a role in stabilizing the dodecamers whereas the one in Rvb2 does not seem to be involved. In this later study, the mutant Rvb1 and Rvb2 proteins contained an N-terminal histidine tag and a C-terminal histidine tag, respectively. Surprisingly, it was also found that the Rvb1/Rvb2 complex assembled from both mutants lacking the insertion domain still showed formation of some dodecamers and hexamers.[18] This result suggests that, in addition to the insertion domains, a secondary motif in the Rvb proteins may also mediate the interaction between the two hexameric rings in the dodecameric structure.

Here, the 3D structures of the dodecamers formed by the histidine-tagged Rvb1 and Rvb2 proteins are in overall good agreement with the previously reported cryo-EM structure of the yeast Rvb1/His-Rvb2 complex shown in Fig. 2c.[17] However, it is surprising that the raw particle images described in this previous study and the ones obtained by us with the analogous complex are somehow different. Torreira *et al.* found that the most prominent view of the Rvb1/His-Rvb2 complex in electron micrographs was suggestive of a four-petal flower. Instead, the most frequent view seen in our images shows barrel-shaped particles (Fig. 4b). In addition, we found that the histidine-tag-induced dodecamers in our study reverted into hexamers upon the removal of the histidine tags. Conversely, Torreira *et al.* indicated that the dodecamers were still visible by size-exclusion chromatography and EM after cleavage of the histidine tag.[17] At this point, it is unclear what may be causing these differences. The two studies used different protein expression systems and complex assembly protocols. Mainly,

Torreira *et al.* expressed and reconstituted the dodecameric complexes *in vivo* by using insect cells. On the other hand, we performed *in vitro* the assembly of the histidine-tagged complexes from purified components expressed in *E. coli*. However, our data clearly establish that the presence of histidine tags has an influence on the oligomeric state of the Rvb but is not affected by the protein expression system or whether the complexes were assembled *in vivo* or *in vitro*. Further investigations should clarify the causes of the observed differences.

In summary, most of the structural works on both human and yeast Rvb proteins have been performed with tagged constructs. However, further studies of these proteins should be performed with untagged Rvb1 and Rvb2 proteins. These experiments will determine which of the described oligomeric forms of the Rvb1/Rvb2 complex are genuine and represent physiological oligomers rather than structures induced by the experimental conditions. Nonetheless, an interesting question that still remains is whether the histidine-tag-induced Rvb dodecamers described herein simply constitute an experimental artifact or somehow possess some resemblance to the oligomeric states that these proteins may adopt naturally upon binding to other protein partners.

Materials and Methods

Protein expression and purification

Both yeast Rvb1 and Rvb2 proteins were expressed as N-terminal His_6-tagged fusion proteins in *E. coli* BL21 (DE3) cells using previously obtained clones of the genes in the pProEX HTb and p11 expression vectors, respectively.[16] For both proteins, cells were grown in LB medium at 37 °C to an OD_{600} of 0.6, and expression was induced with 1 mM IPTG. Cells were induced overnight at 18 °C.

Lysis was performed in 30 mL of lysis buffer [25 mM Tris/HCl (pH 7.5), 0.5 M NaCl, 10 mM imidazole, and 10% (vol/vol) glycerol] by addition of 30 mg of lysozyme, incubation for 30 min on ice, and sonication. The lysate was cleared by centrifugation at 39,000*g* for 40 min and filtered with a 0.22-μm filter. Subsequently, it was loaded into a HiTrap Metal Chelating column (GE Healthcare Life Sciences) equilibrated with lysis buffer. Unspecifically bound proteins were washed with increasing concentrations of imidazole up to 50 mM, and the N-terminal His_6-tagged Rvb1 and Rvb2 were eluted with 250 mM imidazole. Fractions containing the proteins were pooled and dialyzed against 25 mM Tris/HCl (pH 7.5), 40 mM KCl, and 10% (vol/vol) glycerol. In those cases where we aimed to purify the untagged Rvb1 or Rvb2 proteins, TEV protease was used to remove the N-terminal His_6-tag. Then, a 200-μL volume of a 6.5 mg/mL TEV stock solution was added to the pooled fractions containing the protein after the first dialysis buffer exchange, and the mixture was maintained in dialysis for 12 h more. Both untagged and N-terminal His_6-tag proteins were further purified and concentrated by loading the protein mixture into a Q-Sepharose column (GE Healthcare Life Sciences) equilibrated with 25 mM Tris/HCl (pH 7.5), 40 mM KCl, and 10% (vol/vol) glycerol. Washes were performed with increasing concentrations of NaCl up to 80 mM, and the protein was eluted with 25 mM Tris/HCl (pH 7.5), 0.5 M NaCl, and 10% (vol/vol) glycerol. In the purification of untagged Rvb proteins, the fractions from the Q-Sepharose column containing the Rvb proteins were loaded into a second HiTrap Metal Chelating column (GE Healthcare Life Sciences) equilibrated with 25 mM Tris/HCl (pH 7.5), 0.5 M NaCl, 50 mM imidazole, and 10% (vol/vol) glycerol to remove any residual uncleaved Rvb protein. The flow-through of the column containing the untagged Rvb proteins was collected; dialyzed against 25 mM Tris/HCl (pH 7.5), 40 mM KCl, and 10% (vol/vol) glycerol; and further concentrated in a Q-Sepharose column as described above. The fractions containing pure untagged or N-terminal His_6-tag Rvb proteins were finally dialyzed in storage buffer [25 mM Tris/HCl (pH 7.5), 80 mM KCl, and 10% (vol/vol) glycerol].

In vitro assembly and purification of Rvb1/Rvb2 complexes

Untagged and histidine-tagged Rvb1/Rvb2 complexes were assembled in 600 μL of reaction mixtures in assembly buffer [25 mM Tris/HCl (pH 7.5), 80 mM KCl, 10% (vol/vol) glycerol, 1 mM DTT, and 1.5 mM ADP]. Each protein in the reaction had a concentration of 6 μM. The reaction mixtures were incubated at 37 °C for 30 min and loaded into a Superdex 200 10/300 GL column (GE Healthcare Life Sciences) equilibrated in 25 mM Tris/HCl (pH 7.5), 80 mM KCl, and 10% (vol/vol) glycerol at 4 °C and at a flow rate of 0.3 mL/min. The same buffer, but also containing 1.5 mM ADP, was used to equilibrate the column when the untagged Rvb1/Rvb2 complex was loaded. In this case, ADP was required to maintain the integrity of the hexamers. A gel-filtration calibration kit (HMW; GE Healthcare Life Sciences) was used for column calibration.

Complexes to be loaded into native BN-PAGE gels were assembled as described above. However, in this case, the volume of the assembly reactions was only 20 μL. The concentration of each protein in the assembly reactions was 6 μM in the reactions containing both Rvb proteins and 9.5 μM in the samples that had only one of the proteins. The samples were then diluted 4-fold in assembly buffer, and a 15-μL volume of each diluted sample was mixed with 5 μL of loading dye and resolved by BN-PAGE (NativePAGE™ Novex® Bis-Tris Gel System; Invitrogen) following the manufacturer's protocols. In the case of complexes purified by size-exclusion chromatography, 15 μL of each indicated fraction was mixed with 5 μL of loading dye and resolved in the gels.

Purification of the yeast R2TP and endogenous Rvb1/Rvb2 complexes

R0065 yeast cells in W303 background (*MATa leu2-3,112 trp1-1 can1-100 ura3-1 ade2-1 his3-11,15 Pih1-3FLAGKAN*) were grown in 4 L of yeast–peptone–dextrose medium at 30 °C overnight until an OD_{600} of ~1.5–2 had been

reached. Cells were harvested, washed with 5 vol of H_2O, and then washed with 5 vol of buffer H-0.3 [one ethylenediaminetetraacetic-acid-free protease, one inhibitor cocktail tablet (Roche) in 50 mL of 25 mM Hepes–KOH (pH 7.6), 1 mM ethylenediaminetetraacetic acid, 10% glycerol, 0.02% NP-40, 300 mM KCl, 2.5 mM DTT, and 10 mM $MgCl_2$]. Approximately 60 mL of cell pellet was then loaded into syringes and squeezed into liquid nitrogen to generate "noodles." Cell pellets were then broken for 4 min using a coffee grinder. The broken cells were then incubated at room temperature until they were damp but slightly frozen. They were then placed on ice and resuspended with an equal volume of buffer H-0.3. Lysate and cell debris were then separated by centrifugation at 22,000***g*** for 1 h at 4 °C. A 60-mL volume of lysate was collected and mixed with 400 μL of anti-FLAG beads (Sigma), which were washed twice with 5 vol of buffer H-0.5 (same as buffer H-0.3 but containing 500 mM KCl) for 1 h at 4 °C. The beads were centrifuged at 900***g*** for 30 s at 4 °C. The supernatant was then removed, and the beads were washed five times with 10 vol of buffer H-0.5 for 5 min at 4 °C. The beads were then washed three times with 10 vol of buffer H-0.1 (same as buffer H-0.3 but containing 100 mM KCl) for 5 min at 4 °C. Finally, the beads were incubated with 400 μL of ATP buffer (3 mM ATP in 25 mM Tris/HCl, pH 7.5) for 30 min at room temperature, and the supernatant containing untagged endogenous Rvb1/Rvb2 complexes was collected. Instead, the R2TP complexes were eluted with FLAG peptide (Sigma). Both samples were immediately visualized using EM and resolved in a 12% SDS-PAGE gel that was subsequently silver stained.

EM and 3D reconstructions

Samples from sizing column fractions were applied by floating a 10-μL drop on carbon-coated grids that had been previously glow discharged and negatively stained with 1% uranyl acetate. Specimens were observed with a JEOL 2010F electron microscope operated at 200 kV. Images were collected at a magnification of 50,000× at a dose of 10 e/Å^2. All images were recorded on Kodak SO-163 films, scanned on a Nikon Super COOLSCAN 9000 ED at 6.35 μm/pixel, and averaged two times to produce data at 2.54 Å/pixel.

Particles were extracted interactively from digitized fields using the 'Boxer' program (EMAN).[24] Cross-correlation methods in the 'align2d' program (XMIPP)[25] were used to align the ring-shaped and barrel-shaped particles and to obtain the two-dimensional (2D) averages.

To perform a symmetry analysis of ring-shaped particles representing the top views of histidine-tagged complexes, we first translationally aligned the normalized images relative to a previously obtained circularly symmetric reference image produced by averaging all the images in the data set. The presence of statistically significant rotational symmetry in the data was then assessed using two statistical tests, the spectral ratio product and Student's *t* test, as previously described.[20]

The 3D reconstructions were calculated using standard 3D projection-matching procedures, as implemented in the XMIPP software package.[25] Two initial references were used. The first one was built using the 'startcsym' program (EMAN)[24] and 6-fold rotational symmetry. The second reference was produced from the previously published double hexameric ring structure of the yeast Rvb1/His-Rvb2 complex.[17] The two initial references had been low-pass filtered to 30 Å before their 2D projections were calculated to initiate the projection-matching procedure. The resulting maps were low-pass filtered to their estimated resolution using a Fourier shell correlation value of 0.5.

Docking of X-ray crystallographic structures, model generation, and structure visualization

Fitting of the X-ray structure of the human Rvb1 hexamer [Protein Data Bank (PDB) ID 2C9O] onto the EM maps of the histidine-tagged Rvb1/Rvb2 complexes was performed using rigid-body fitting. The AAA^+ core domain (residues 9–119 and 296–449) and the globular part of the insertion domain (residues 130–231) were docked independently. In each case, the X-ray model was first manually docked onto the EM map, and the fitting was then optimized using the 'Fit in Map' option in Chimera.[26] The DII–DII, AAA–AAA, and AAA–DII models generated were transformed into density maps, and their side-view projections were calculated using the 'pdb2mrc' and 'project3d' programs (EMAN),[24] respectively. Visualization of the EM density maps, fitted atomic structures, and constructed models was performed with UCSF Chimera software.

Accession numbers

The EM maps of the singly and doubly histidine-tagged Rvb1/Rvb2 complexes have been deposited in the Electron Microscopy Data Bank (EMDB) (EMDB IDs 5228, 5229, and 5230).

Acknowledgements

We are grateful to the staff at the Canadian Center for Electron Microscopy. J.H. holds a Natural Sciences and Engineering Research Council of Canada PGSD2 fellowship. Our work in this field was supported by a Discovery grant from the National Science and Engineering Research Council of Canada (RGPIN288327-07 to J.O.) and by the Canadian Institutes of Health Research (MOP-93778 to W.A.H.).

Supplementary Data

Supplementary data to this article can be found online at doi:10.1016/j.jmb.2010.10.003

References

1. Kanemaki, M., Makino, Y., Yoshida, T., Kishimoto, T., Koga, A., Yamamoto, K. *et al.* (1997). Molecular

cloning of a rat 49-kDa TBP-interacting protein (TIP49) that is highly homologous to the bacterial RuvB. *Biochem. Biophys. Res. Commun.* **235**, 64–68.
2. Kanemaki, M., Kurokawa, Y., Matsu-ura, T., Makino, Y., Masani, A., Okazaki, K. *et al.* (1999). TIP49b, a new RuvB-like DNA helicase, is included in a complex together with another RuvB-like DNA helicase, TIP49a. *J. Biol. Chem.* **274**, 22437–22444.
3. Wood, M. A., McMahon, S. B. & Cole, M. D. (2000). An ATPase/helicase complex is an essential cofactor for oncogenic transformation by c-Myc. *Mol. Cell*, **5**, 321–330.
4. Jin, J., Cai, Y., Yao, T., Gottschalk, A. J., Florens, L., Swanson, S. K. *et al.* (2005). A mammalian chromatin remodeling complex with similarities to the yeast INO80 complex. *J. Biol. Chem.* **280**, 41207–41212.
5. Jonsson, Z. O., Jha, S., Wohlschlegel, J. A. & Dutta, A. (2004). Rvb1p/Rvb2p recruit Arp5p and assemble a functional Ino80 chromatin remodeling complex. *Mol. Cell*, **16**, 465–477.
6. Mizuguchi, G., Shen, X., Landry, J., Wu, W. H., Sen, S. & Wu, C. (2004). ATP-driven exchange of histone H2AZ variant catalyzed by SWR1 chromatin remodeling complex. *Science*, **303**, 343–348.
7. Shen, X., Mizuguchi, G., Hamiche, A. & Wu, C. (2000). A chromatin remodelling complex involved in transcription and DNA processing. *Nature*, **406**, 541–544.
8. Newman, D. R., Kuhn, J. F., Shanab, G. M. & Maxwell, E. S. (2000). Box C/D snoRNA-associated proteins: two pairs of evolutionarily ancient proteins and possible links to replication and transcription. *RNA*, **6**, 861–879.
9. Watkins, N. J., Dickmanns, A. & Luhrmann, R. (2002). Conserved stem II of the box C/D motif is essential for nucleolar localization and is required, along with the 15.5K protein, for the hierarchical assembly of the box C/D snoRNP. *Mol. Cell. Biol.* **22**, 8342–8352.
10. Watkins, N. J., Lemm, I., Ingelfinger, D., Schneider, C., Hossbach, M., Urlaub, H. & Luhrmann, R. (2004). Assembly and maturation of the U3 snoRNP in the nucleoplasm in a large dynamic multiprotein complex. *Mol. Cell*, **16**, 789–798.
11. Zhao, R., Kakihara, Y., Gribun, A., Huen, J., Yang, G., Khanna, M. *et al.* (2008). Molecular chaperone Hsp90 stabilizes Pih1/Nop17 to maintain R2TP complex activity that regulates snoRNA accumulation. *J. Cell Biol.* **180**, 563–578.
12. Gartner, W., Rossbacher, J., Zierhut, B., Daneva, T., Base, W., Weissel, M. *et al.* (2003). The ATP-dependent helicase RUVBL1/TIP49a associates with tubulin during mitosis. *Cell Motil. Cytoskeleton*, **56**, 79–93.
13. Sigala, B., Edwards, M., Puri, T. & Tsaneva, I. R. (2005). Relocalization of human chromatin remodeling cofactor TIP48 in mitosis. *Exp. Cell Res.* **310**, 357–369.
14. Matias, P. M., Gorynia, S., Donner, P. & Carrondo, M. A. (2006). Crystal structure of the human AAA^+ protein RuvBL1. *J. Biol. Chem.* **281**, 38918–38929.
15. Puri, T., Wendler, P., Sigala, B., Saibil, H. & Tsaneva, I. R. (2007). Dodecameric structure and ATPase activity of the human TIP48/TIP49 complex. *J. Mol. Biol.* **366**, 179–192.
16. Gribun, A., Cheung, K. L., Huen, J., Ortega, J. & Houry, W. A. (2008). Yeast Rvb1 and Rvb2 are ATP-dependent DNA helicases that form a heterohexameric complex. *J. Mol. Biol.* **376**, 1320–1333.
17. Torreira, E., Jha, S., Lopez-Blanco, J. R., Arias-Palomo, E., Chacon, P., Canas, C. *et al.* (2008). Architecture of the pontin/reptin complex, essential in the assembly of several macromolecular complexes. *Structure*, **16**, 1511–1520.
18. Niewiarowski, A., Bradley, A. S., Gor, J., McKay, A. R., Perkins, S. J. & Tsaneva, I. R. (2010). Oligomeric assembly and interactions within the human RuvB-like RuvBL1 and RuvBL2 complexes. *Biochem. J.* **429**, 113–125.
19. Cheung, K. L., Huen, J., Houry, W. A. & Ortega, J. (2010). Comparison of the multiple oligomeric structures observed for the Rvb1 and Rvb2 proteins. *Biochem. Cell Biol.* **88**, 77–88.
20. Kocsis, E., Cerritelli, M. E., Trus, B. L., Cheng, N. & Steven, A. C. (1995). Improved methods for determination of rotational symmetries in macromolecules. *Ultramicroscopy*, **60**, 219–228.
21. Ludtke, S., He, K. & Huang, H. (1995). Membrane thinning caused by magainin 2. *Biochemistry*, **34**, 16764–16769.
22. Zhao, R. & Houry, W. A. (2005). Hsp90: a chaperone for protein folding and gene regulation. *Biochem. Cell Biol.* **83**, 703–710.
23. Ortega, J., Singh, S. K., Ishikawa, T., Maurizi, M. R. & Steven, A. C. (2000). Visualization of substrate binding and translocation by the ATP-dependent protease, ClpXP. *Mol. Cell*, **6**, 1515–1521.
24. Ludtke, S. J., Baldwin, P. R. & Chiu, W. (1999). EMAN: semiautomated software for high-resolution single-particle reconstructions. *J. Struct. Biol.* **128**, 82–97.
25. Scheres, S. H., Nunez-Ramirez, R., Sorzano, C. O., Carazo, J. M. & Marabini, R. (2008). Image processing for electron microscopy single-particle analysis using XMIPP. *Nat. Protoc.* **3**, 977–990.
26. Pettersen, E. F., Goddard, T. D., Huang, C. C., Couch, G. S., Greenblatt, D. M., Meng, E. C. & Ferrin, T. E. (2004). UCSF Chimera—a visualization system for exploratory research and analysis. *J. Comput. Chem.* **25**, 1605–1612.

SUPPLEMENTARY DATA

Alternative Oligomeric States of the Yeast Rvb1/Rvb2 Complex Induced by Histidine Tags

Kevin L. Y. Cheung, Jennifer Huen, Yoshito Kakihara, Walid A. Houry and Joaquin Ortega

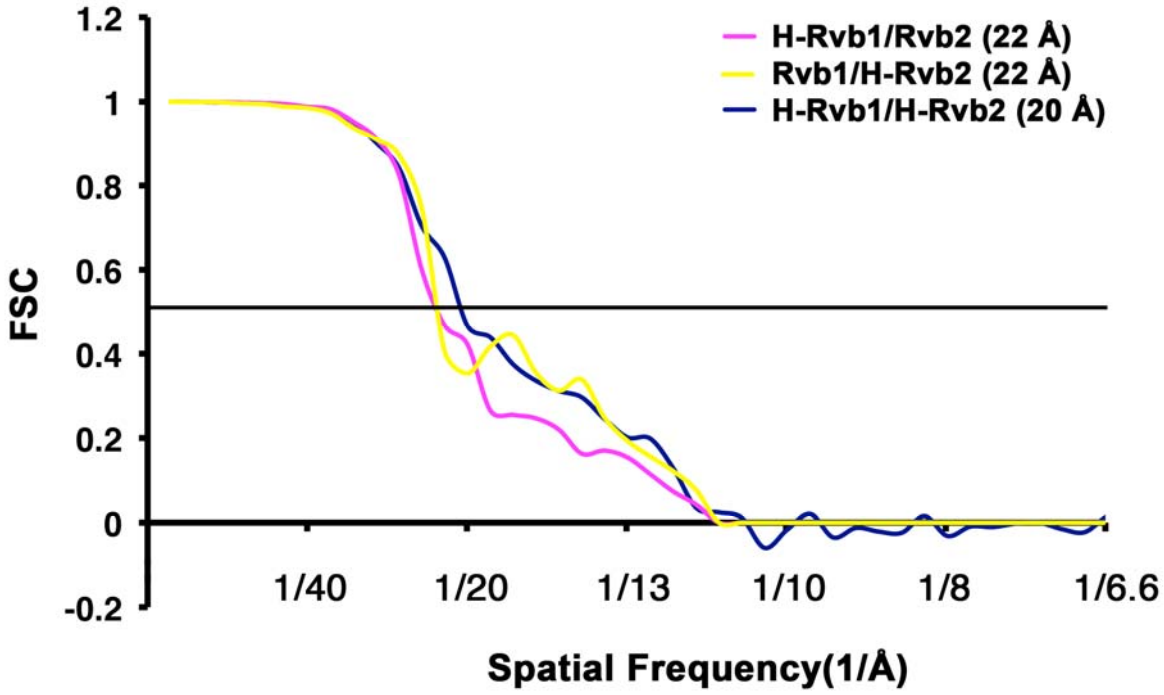

Fig. S1. Estimation of the resolution of the three-dimensional reconstruction of the histidine tagged Rvb1/Rvb2 complexes.

Fourier Shell Correlation (FSC) plots corresponding to the three-dimensional reconstructions of the His-Rvb1/Rvb2 (H-Rvb1/Rvb2), Rvb1/His-Rvb2 (Rvb1/H-Rvb2) and His-Rvb1/His-Rvb2 (H-Rvb1/H-Rvb2). The estimated resolution for the three maps using a FSC value of 0.5 (horizontal line) is indicated next to the corresponding label between brackets.

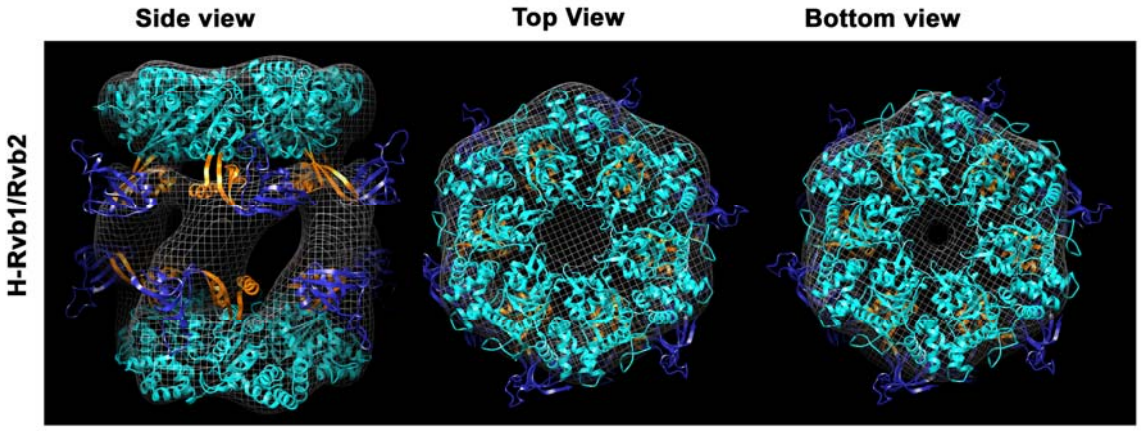

Fig. S2. Docking of the complete X-ray structure of the human Rvb1 hexamer into the three-dimensional reconstruction of the histidine tagged Rvb1/Rvb2 complexes. The panel shows the fitting of the X-ray structure of human Rvb1 hexamer (PDB 2C9O) in the conformation displayed in the X-ray crystal structure into the three-dimensional reconstruction of His-Rvb1/Rvb2 (H-Rvb1/Rvb2) complex. The insertion domains of the Rvb1 protein clearly protrude outside the EM density map of the histidine tagged complex. Human Rvb1 hexamer is displayed as a ribbon representation color coded as in Fig. 1 with AAA+ core domains of the monomers colored in cyan, the globular part of the insertion domain colored in blue and the linker region between these two domains colored in orange. The EM density map is shown as a mesh.

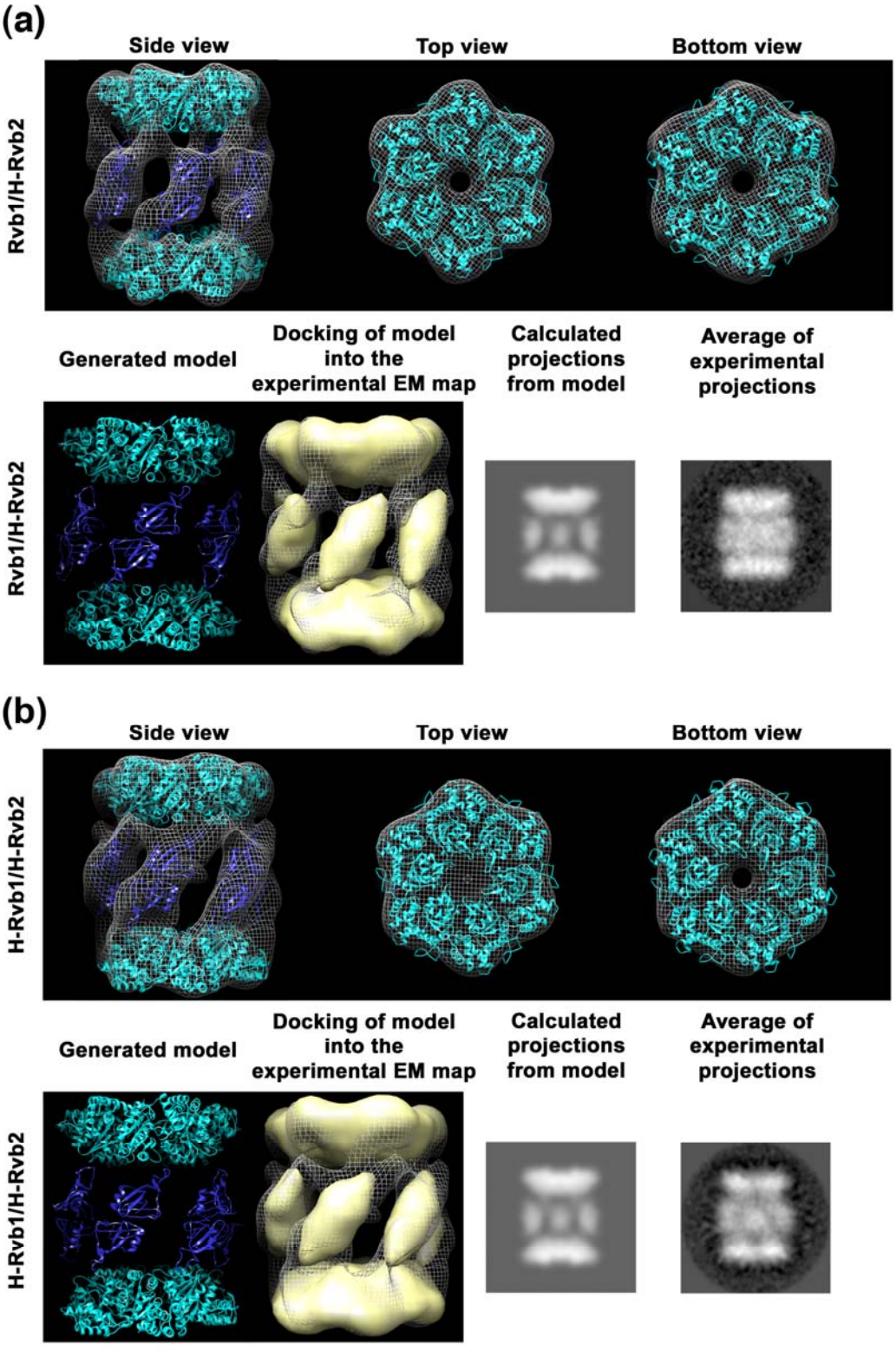
(a)
Side view
Top view
Bottom view
Rvb1/H-Rvb2
Generated model
Docking of model into the experimental EM map
Calculated projections from model
Average of experimental projections
Rvb1/H-Rvb2
(b)
Side view
Top view
Bottom view
H-Rvb1/H-Rvb2
Generated model
Docking of model into the experimental EM map
Calculated projections from model
Average of experimental projections
H-Rvb1/H-Rvb2

Fig. S3. Docking of the X-ray structure of the human Rvb1 hexamer into the three-dimensional reconstruction of the histidine tagged Rvb1/His-Rvb2 and His-Rvb1/His-Rvb2 complexes.

The upper panels in (a) and (b) show the fitting of the AAA+ core domain and globular part of the insertion domains of the crystal structure of human Rvb1 into the three-dimensional reconstructions of the histidine tagged Rvb1/His-Rvb2 (Rvb1/H-Rvb2) and His-Rvb1/His-Rvb2 (H-Rvb1/H-Rvb2) complexes, respectively. The AAA+ and insertion domains are shown as a ribbon representation color coded as in Fig. 1 and prepared from PDB file 2C9O. The EM density map of the Rvb1/His-Rvb2 and His-Rvb1/His-Rvb2 complexes is shown as a mesh.

The left column in the lower panels of (a) and (b) shows the DII-DII models generated by fitting the crystal structure of human Rvb1 into the three-dimensional reconstruction of the Rvb1/His-Rvb2 and His-Rvb1/His-Rvb2 EM maps, respectively. The AAA+ and insertion domains are shown as a ribbon representation color coded as in Fig. 1 and prepared from PDB file 2C9O. The second column from the left shows the surface rendering representation of the density maps generated from the models fitted into the density map of the three dimensional reconstruction of the corresponding complex represented as a mesh. The third column from the left shows the calculated side view projections from the models and the right column displays an average of experimental projections from the corresponding complex obtained from negatively stained electron micrographs.

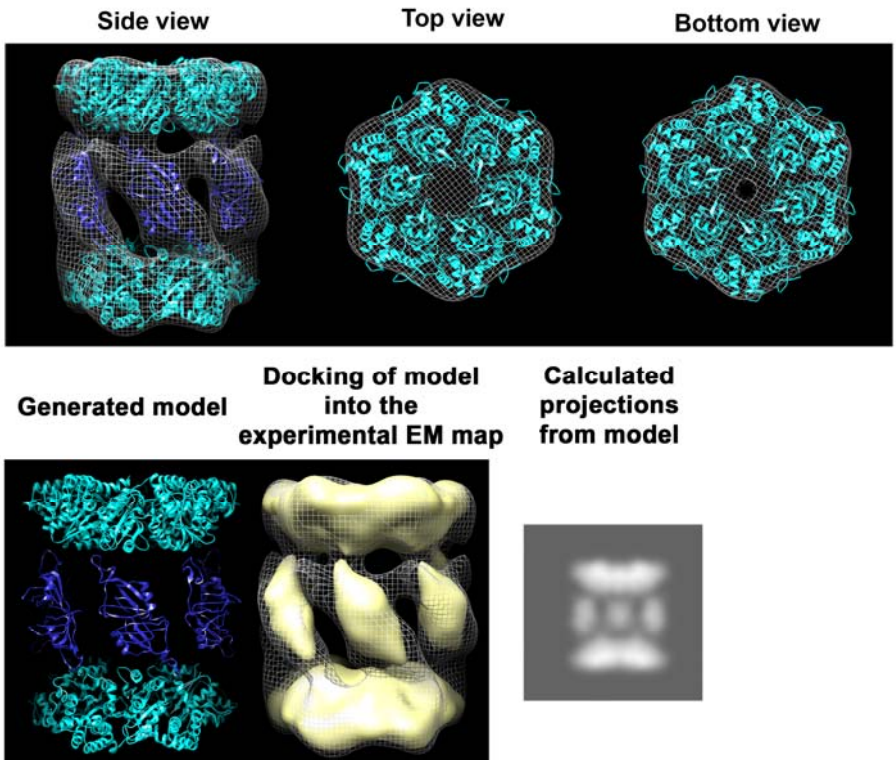

Fig. S4. Docking of the X-ray structure of the human Rvb1 hexamer into the three-dimensional reconstruction of the histidine tagged His-Rvb1/Rvb2 complex with opposite handedness.

Fitting of the AAA+ core domain and globular part of the insertion domains of the crystal structure of human Rvb1 into the three-dimensional reconstructions of the histidine tagged His-Rvb1/ Rvb2 complex with opposite handedness to the one shown in Fig. 5. The AAA+ and insertion domains are shown as a ribbon representation color coded as in Fig. 1 and prepared from PDB file 2C9O. The EM density map of the complex is shown as a mesh. In the lower panel the left column shows the DII-DII model generated from this EM map. The middle column shows the surface rendering representation of the density map generated from the model fitted into the density map of the His-Rvb1/His-Rvb2 complex with opposite handedness. The right column shows the calculated side view projections from the density map of the model.

Supplementary Table 1. Analysis of the rotational symmetry of the ring-shaped particles from histidine tagged Rvb1/Rvb2 complexes.

Complex	Number of particles analized	Symmetry dectected	*t* test and significance level (*p*)	Spectral ratio product
H-Rvb1/Rvb2	305	6	<0.000001	3.88×10^{10}
Rvb1/H-Rvb2	205	6	<0.000001	3.62×10^{45}
H-Rvb1/H-Rvb2	71	6	<0.000001	3.48×10^{7}